Synthesis of porous CuO/Cu_2O composite microsphere and its visible-light photocatalytic degradation for dye pollutions

XIAOYAN GAO[a,b], WEIGANG DU[a], DONG LI[a], KUN HONG[a,b], XIAOJIE ZHANG[a,b,c,*]
[a]*National & Local Joint Engineering Research Center for Mineral Salt Deep Utilization, Huaiyin Institute of Technology, Huaian 223003, China*
[b]*Key Laboratory for Palygorskite Science and Applied Technology of Jiangsu, Huaiyin Institute of Technology, Jiangsu Province, Huaian 223003, P. R. China*
[c]*School of Electrical and Power Engineering, China University of Mining and Technology, Xuzhou 221116, China*

In this work, porous CuO/Cu_2O composite microspheres were prepared with a simple hydrothermal method. The porous CuO/Cu_2O composite microsphere was applied for photodegradation of methylene orange (MO) under visible light irradiation with the synergistic effect of H_2O_2 and showed good photocatalytic performance to degrade the MO (100 % with the irradiation time of 70 min). The improved photocatalytic properties of CuO/Cu_2O may be ascribed to the formation of p-n heterojunctions between CuO and Cu_2O, resulting in the effective separation of photogenerated electron-hole pairs and the enhanced absorption of visible light.

(Received May 21, 2019; accepted June 16, 2020)

Keywords: CuO/Cu_2O composite photocatalyst, Heterojunctions, Visible-light irradiation, Photocatalytic degradation

1. Introduction

Organic contaminations, especially industrial dye pollutants have become a serious environmental problem [1]. Due to the complex molecular structures of dye, which make them stable and difficult to degrade. Among the methods to remove dye compounds in water, advanced oxidation processes (AOPs) have displayed many advantages such as high efficiency, energy economic and zero waste [2-5].

Over the past decade, semiconductor photocatalytic technology as one of efficient AOPs, has aroused great attention owing to their intriguing potential for various applications, such as the current energy and environmental problems. However, most of the photocatalysts are hampered in the application due to their absorption of UV light, which is only about 4% in the sunlight [6-8]. Therefore, development of the photocatalysts with absorption of visible light and excellent performance, low cost is emergency. Among various metal oxides, copper oxide compounds, with respect to commercial production, appear to be more advantageous when compared with conventional photocatalysts owing to their highlighted superiorities such as high abundance, simple preparation, low cost, and environmental friendliness [9-12]. For instance, CuO and Cu_2O feature small band gaps (Eg (CuO) = 1.2 eV and Eg (Cu_2O) = 2.0 eV) for visible-light absorption without the decoration of any photo-sensitizers. It is well known that the performance of the materials is closely related to their composition, [13] morphology, [14] and structure, [11, 15] etc. Thus, many CuO and Cu_2O with different shapes such as polyhedral, hierarchical, hollow structures have been prepared with different methods [10, 16-19]. In addition, recent studies exhibit that bi-component metal oxides, integrating two types of functional materials, often exhibit a strong synergistic effect, resulting in an increasing property [12, 16, 20, 21].

Herein, a facile and green synthesis method was explored to prepare the porous bi-component copper oxides CuO/Cu_2O. The as prepared CuO/Cu_2O composites was employed for oxidative degradation of organic dye pollutants under visible light irradiation. It was demonstrated that porous CuO/Cu_2O composites micro/nano structure exhibited enhanced photocatalytic oxidation activity of dye molecules.

2. Experimental

The microsphere was obtained by the hydrothermal method according to previous report [11, 22]. All the reagents used were analytical grade and used without further purification. In a typical procedure, the pH of $Cu(NO_3)_2$ solution (0.1 mol l^{-1}) was adjusted with ammonia solution (25 %) to about 11, and then stirred at 60 °C for 30 min. After that 15 μl hydrazine (35 wt.%) was

added into the above mixture solution. The solution mixture was transferred to a Teflon-lined stainless steel autoclave which was then heated at 120 °C for 24 h in an electric oven. Finally, the black precipitate was separated from the reaction mixture by centrifugation, and washed several times with distilled water. The product was dried at 100 °C for further use.

The morphology and structure of as-synthesized samples were characterized by field emission scanning electron microscopy (FESEM, Hitachi S-4800), transmission electron microscopy (TEM, JEOL-2010) and X-ray diffraction (XRD, Holland Panalytical PRO PW 3040/60) with Cu Kα radiation (V = 30 kV, I = 25 mA, λ = 1.5418 Å). The specific surface areas of the samples were calculated from the nitrogen adsorption/desorption isotherms (Micromeritics, ASAP 2020 at 77 K) based the Brunauer-Emmett-Teller (BET) method and the corresponding pore size distribution was deduced from the adsorption segments using Barret-Joyner-Halenda (BJH) method. X-ray photoelectron spectroscopy (XPS) data were collected from a VG (ESCALAB210) multifunctional X-ray photoelectron spectrometer to analyze the surface elements of the samples (the used source type: Al Kα, hv = 1486.6 eV, power: 150W, 50μm, BE reference(s): C1s 284.8 eV, pass energy: 100 eV, energy/step: 1eV/0.05eV).

The photocatalytic activities of the catalysts were monitored by degradation methyl orange (MO) under visible light irradiation at room temperature. In a typical reaction, 30 mg of photocatalyst power was dispersed into 50 ml of dye solution (20 mg l^{-1}) with addition of 0.05 ml H_2O_2 solution (10 wt %). In order to reach adsorption/desorption equilibrium of dye molecules on the photocatalyst, the suspension was stirred at dark for 30 min before the irradiation of 500 W Xe arc lamp and the light tough a UV cutoff filter (λ > 420 nm). At different irradiation time intervals, the suspensions were collected, and then immediately centrifuged to remove the photocatalyst particles. The concentrations of MO were tested with a UV-vis spectrophotometer (Hitachi, UV-3310) by measuring the characteristic absorption peak intensity at 465 nm. The degradation rate of MO is defined as the following equation: D (%) = $(C_0\text{-}C)/C_0$ * 100 %, where C_0 and C are the concentrations of the initial and the certain time (t) of the MO.

3. Results and discussion

The XRD pattern results indicate the presence of two CuO and Cu_2O phases in the prepared product, all the peaks could be indexed to the monoclinic symmetry of CuO (JCPDS No. 05-0661) and cubic phase Cu_2O (JCPDS No. 05-0667). The average particle size of the sample was calculated ca. 30 nm using the Debye-Scherrer formula which is derived from FWHM of the diffraction peaks. In addition, the percentage of CuO and Cu_2O in the microsphere are about 78% and 22% according to normalization method from XRD results.

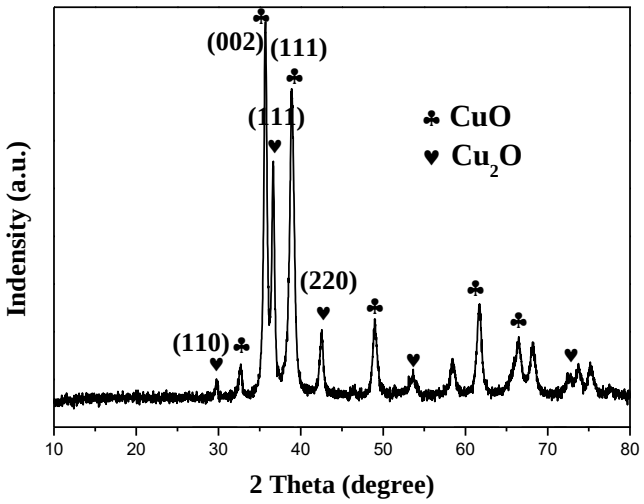

Fig. 1. The XRD pattern of porous CuO/Cu_2O composite microsphere

The general morphologies of the as prepared porous CuO/Cu_2O composite microspheres were examined by SEM, as shown in Fig. 2(a) and (b). The product is composed of microspheres in a diameter range of 2-4 μm. High-magnification SEM image (Fig. 2b) displays that the shell wall of the hollow microspheres is composed of nanoparticles with a diameter of ca. 30-50 nm. The corresponding TEM image (Fig. 2c and d) clearly shows a hollow porous microsphere, which is consistent with the SEM observation. The corresponding selected area electron diffraction pattern (Fig. 3) of the as prepared product is composed of polycrystalline diffraction rings. The interplanar spacing of 0.236 nm and 0.316 nm correspond to the CuO (002) and Cu_2O (111) reflection.

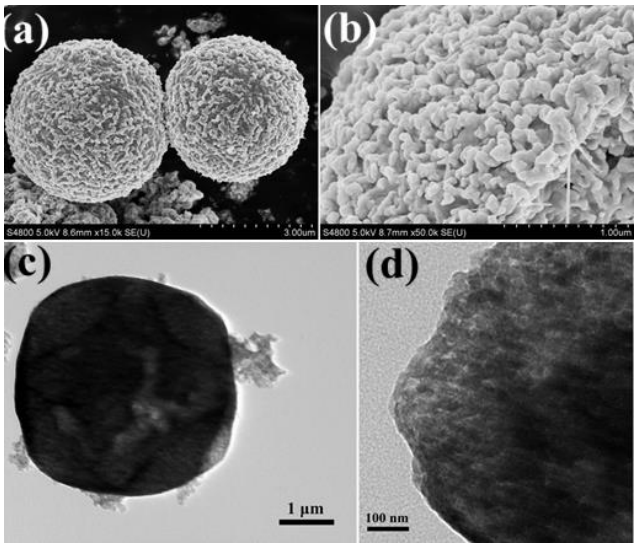

Fig. 2. The SEM (a, b) and TEM (c, d) images of CuO/Cu_2O

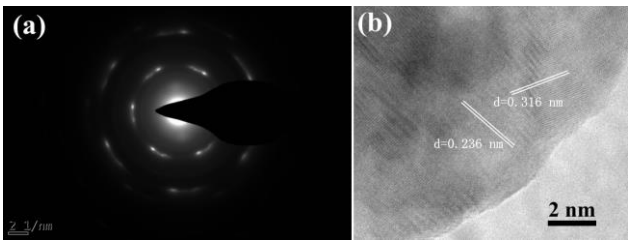

Fig. 3. The selected area electron diffraction pattern (a) and interplanar spacing (b) of CuO/Cu_2O composite microsphere

The N_2 adsorption/desorption isotherm of the as-synthesized porous CuO/Cu_2O microsphere belongs to type IV with a combination of H1 and H3 hysteresis loop, which is a characteristic of mesoporous materials, as shown in Fig. 4. The BET investigation of the product provides a surface area of about 60.2 m^2 g^{-1}, and the pore volume 0.18 cm^3 g^{-1}, average pore diameter 5.9 nm.

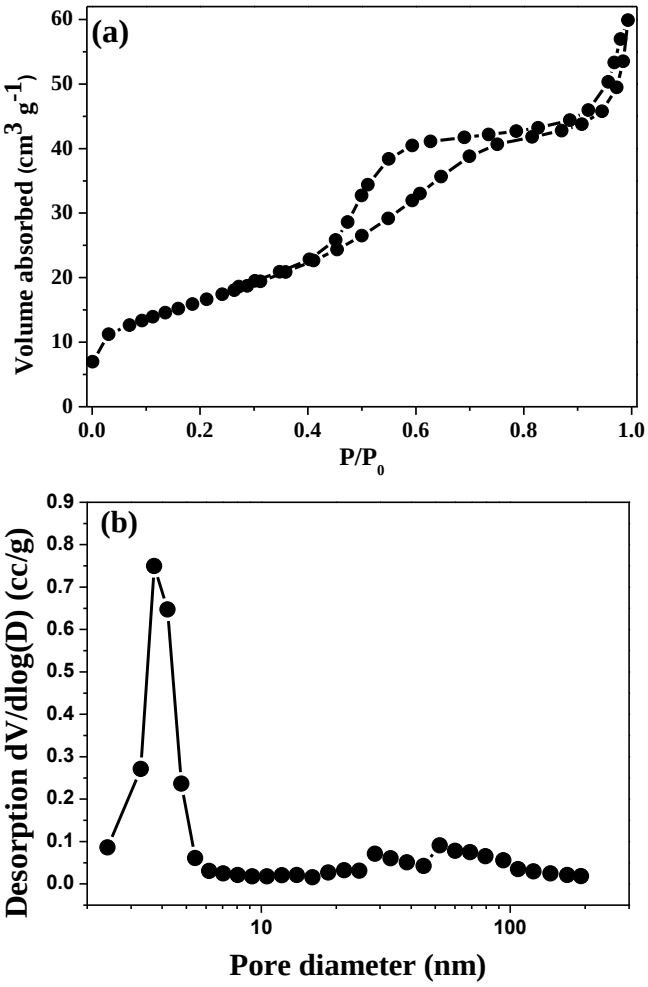

Fig. 4. The N_2 adsorption/desorption isotherm (a) and pore diameter distribution (b) of porous CuO/Cu_2O composite microsphere

X-ray photoelectron spectroscopy (XPS) measurements of porous CuO/Cu_2O microsphere was carried out to confirm the chemical states of elements, and the survey spectrum is presented in Fig. 5(a). Fig. 5(b) shows the high-resolution spectrum of the Cu2p peaks centered at 933.45 eV and 953.5 eV, which belong to Cu2p 3/2 and Cu2p 1/2, respectively [23, 24]. Based on the analysis of the area of XPS peaks for the corresponding peak area shows that Cu(II) is dominant, indicating that the main form of Cu is CuO, while the proportion of Cu(I) is about 20%, which is also consistent with the XRD analysis [25-27].

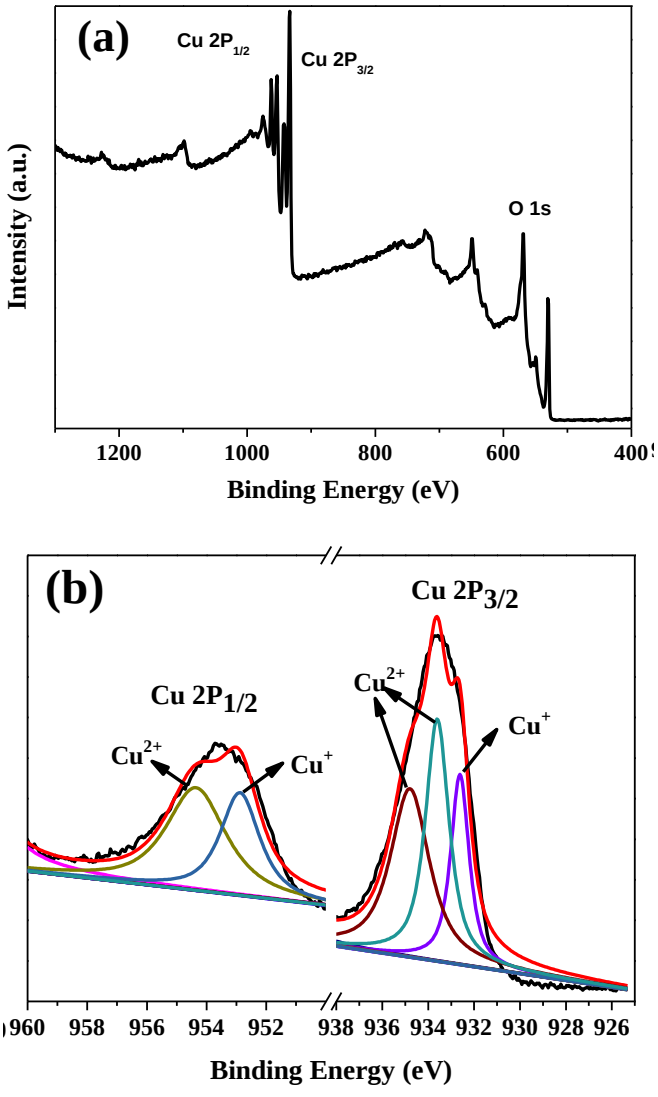

Fig. 5. (a) XPS spectra and (b) the high-resolution spectrum of the Cu2p for CuO/Cu_2O composite microsphere (color online)

Fig. 6 shows the photocatalytic performances of CuO/Cu_2O for degradation of MO at under different conditions. The photocatalytic capacity is very low (about 10 %) without CuO/Cu_2O composite photocatalyst. While it should be noted that in the absence of H_2O_2, the porous

CuO/Cu_2O composite hollow microspheres show weak photocatalytic activities under visible light irradiation. Whereas in presence of H_2O_2, the concentration of MO shows a faster decrease (black line in Fig. 6(a)), suggesting the best degradation rate. The degradation rate is much higher than the previous reports, it can be deduced that the composite of CuO and Cu_2O may be beneficial in reducing the recombination of photogenerated electrons and holes and thus enhances photocatalytic performance. After irradiation for 70 min, the degradation efficiency can be reach to 98%. The interface between the CuO and Cu_2O might act as a rapid separation site for the photogenerated electrons and holes because of the difference in the energy levels of their conduction bands and valence bands.

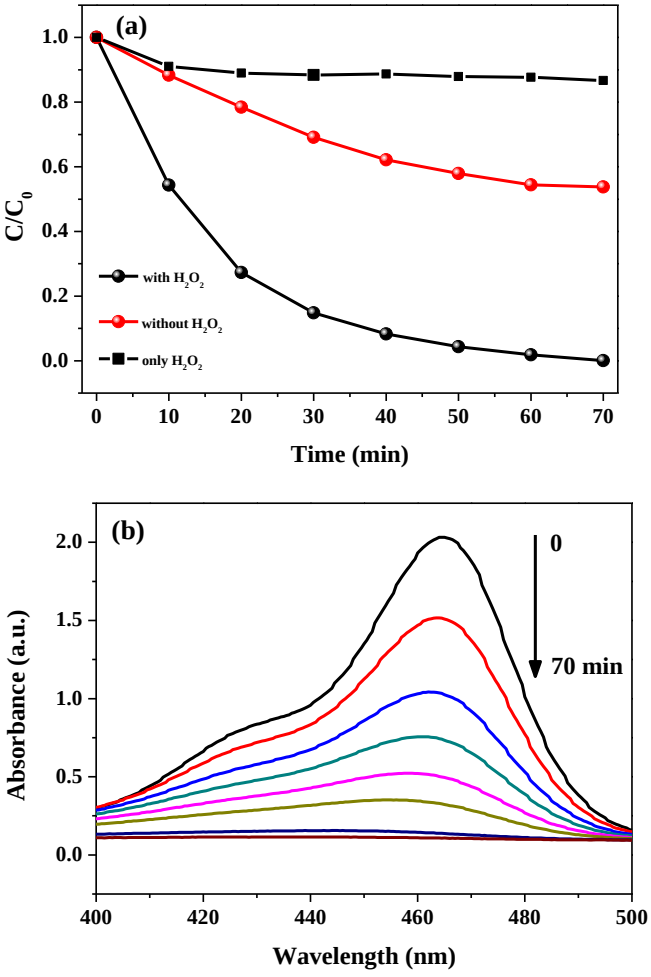

Fig. 6 (a) The photocatalytic degradation performance of CuO/Cu_2O and (b) the absorbance spectra of MO at different times with visible-light irradiation (color online)

The stability of the heterojunction photocatalyst was carried out by repeating experiments on the degradation of MO under visible light irradiation with adding H_2O_2, using porous CuO/Cu_2O composite microspheres. In each test, the photocatalyst was reused after washing by simple filtration followed by ultrasonic cleaning with a mixture of 30% alcohol in water, then drying at 100 °C for 3 h. As shown in Fig. 7, the photocatalytic activity does not exhibit distinct loss after five successive cycles, while the slight loss of photocatalytic efficiency should be described that the active sites are occupied with organic molecular, and the proportion is very low. It suggested that the porous CuO/Cu_2O composite microspheres possesses excellent long-time stability and is not photo-corroded during the photocatalytic degradation of MO under visible light irradiation.

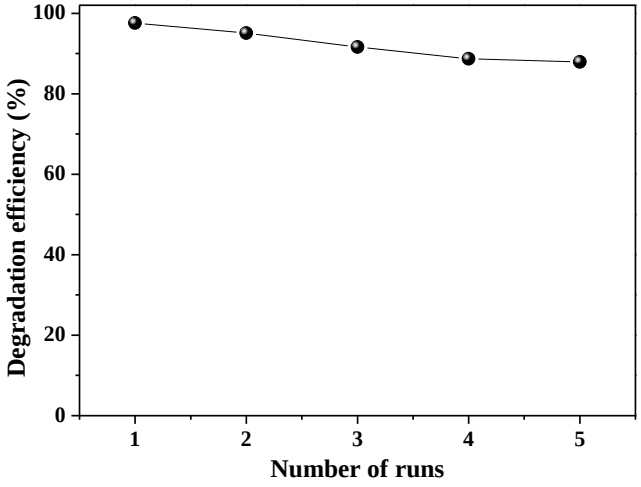

Fig. 7. Recycling tests for the photocatalytic of MO over CuO/Cu_2O

Accordingly, a possible enhanced photocatalytic mechanism for the degradation of MO over porous CuO/Cu_2O composite microspheres can be proposed. When CuO particles are combined with Cu_2O, the p-n type heterojuctions are formed. And there is an internal field presented with the direction from n-type Cu_2O to p-type CuO at the thermodynamic equilibrium of p–n heterojunction semiconductors, which is favorable for the separation of photo-induced electron-hole pairs. Fig. 8 displays the charge transfer pathway in CuO/Cu_2O heterostructures. After visible-light irradiation, the photo-induced electrons on the CB of CuO would be transferred to the CB of Cu_2O, as the photogenerated holes in the VB of Cu_2O would be transferred to the VB of CuO [28, 29]. The electric field at the interface favors the migration of electrons from the VB of the p-type to that of the n-type semiconductor. These would lead to the aggregation of photogenerated electrons on the surface of CuO and photogenerated holes on the surface of Cu_2O. The holes can directly oxidize MO molecules, and the electrons would generate the reductive reaction of H_2O_2, which in favor of the oxidization reaction of MO.

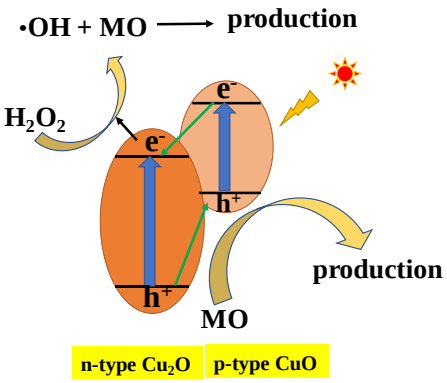

Fig. 8. Proposed possible reaction mechanism for the photocatalytic degradation of MO (color online)

4. Conclusion

Porous CuO/Cu_2O composite microspheres with nanostructure have been synthesized successfully by simple method without using a template. The photocatalytic activity of as-synthesized CuO/Cu_2O composite was investigated on degradation of MO. In addition, experimental results showed that the photocatalysts were easily recovered and reused five times without much loss of activity. The results indicate that porous CuO/Cu_2O composite microspheres is a very efficient photocatalyst under visible light irradiation with H_2O_2, which may be useful in waste water treatment. Moreover, this study provided a cost-effective and convenient synthetic strategy for a heterogeneous photocatalyst, ultimately guiding the brand new perspectives for photocatalytic research.

Acknowledgements

This work was supported by the fund of Key Laboratory for Palygorskite Science and Applied Technology of Jiangsu (HPK201805), Doctoral Fund of Ministry of Education of China (No.2018M642356), the initiate fund of Huaiyin Institute of Technology (Z301B18545, Z301B19512), National & Local Joint Engineering Research Center for Mineral Salt Deep Utilization (SF201907), Qing Lan Project of Jiangsu Province, "333 high level talents training project" of Jiangsu province and "Six Talent Peak" high-level talents of Jiangsu Province.

References

[1] G. Mamba, M. A. Mamo, X. Y. Mbianda, A. K. Mishra, Ind. Eng. Chem. Res. **53**, 14329 (2014).
[2] G. Mamba, X. Y. Mbianda, A. K. Mishra, Mater. Res. Bull. **75**, 59 (2016).
[3] X. Li, T. Xia, C. Xu, J. Murowchick, X. Chen, Catalysis Today **225**, 64 (2014).
[4] N. Mukherjee, B. Show, S. K. Maji, U. Madhu, S. K. Bhar, B. C. Mitra, G. G. Khan, A. Mondal, Mater. Lett. **65**, 3248 (2011).
[5] M. Rabbani, R. Rahimi, M. Bozorgpour, J. Shokraiyan, S. S. Moghaddam, Mater. Lett. **119**, 39 (2014).
[6] J. A. Rengifo-Herrera, J. Kiwi, C. Pulgarin, J. Photoch. Photobio. A **205**, 109 (2009).
[7] P. Basnet, E. Anderson, Y. Zhao, ACS Appl. Mater. Inter. **2**, 2446 (2019).
[8] R. C. Ding, Y. Z. Fan, G. S. Wang, Chemistry Select **3**, 1682 (2018).
[9] S. Q. Lanbing Liu, Jingjing Wang, Wenjing Zheng, Xinwen Du, Chem. Commun. **51**, 5660 (2015).
[10] R. Liu, J. Yin, W. Du, F. Gao, Y. Fan, Q. Lu, Eur. J. Inorg. Chem. **2013**, 1358 (2013).
[11] R. C. D. A. P. B. Pangkita Deka, New J. Chem. **40**, 348 (2016).
[12] R. C. Yang, Z. H. Zhang, Y. M. Ren, X. Zhang, Z. M. Chen, M. D. Xu, Mater. Sci. Tech. **31**, 25 (2015).
[13] J. Y. Huogen Yu, Shengwei Liu, Stephen Mann, Chem. Mater. **19**, 4327 (2007).
[14] W.-C. Huang, L.-M. Lyu, Y.-C. Yang, M.H. Huang, J. Am. Chem. Soc. **134**, 1261 (2012).
[15] L. Li, K. S. Lee, L. Lu, Funct. Mater. Lett. **07**, 1430002 (2014).
[16] X. Xu, Z. Gao, Z. Cui, Y. Liang, Z. Li, S. Zhu, X. Yang, J. Ma, ACS Appl. Mater. Inter. **8**, 91 (2016).
[17] Q. Wang, H. Xu, W. Huang, Z. Pan, H. Zhou, Journal of Hazardous Materials **364**, 499 (2019).
[18] P. Li, L. Liu, D. Qin, C. Luo, G. Li, J. Hu, H. Jiang, W. Zhang, Journal of Materials Science **54**, 2876 (2019).
[19] J. S. Kumar, M. Naresh Chandra, B. Amit, R. S. Ganesh, I. Hiroshi, K. Tapas, Materials Research Express **6**, 025045 (2019).
[20] Y. Li, X. Chen, L. Li, RSC Adv. **9**, 33395 (2019).
[21] P. Liu, R. Bao, D. Fang, J. Yi, L. Li, Adv. Powder Tech. **29**, 2027 (2018).
[22] C. Z. Lili Feng, Guo Gao, Daxing Cui, Nanoscale Res. Lett. **7**, 276 (2012).
[23] S. Aleksandra, K. Kamila, K. Sylwia, R. Artur, Mater. Res. Express **5**, 126406 (2018).
[24] K. Kaviyarasan, V. Vinoth, T. Sivasankar, A. M. Asiri, J. J. Wu, S. Anandan, Ultrasonics Sonochem. **51**, 223 (2019).
[25] C. Lai, M. Zhang, B. Li, D. Huang, G. Zeng, L. Qin, X. Liu, H. Yi, M. Cheng, L. Li, Z. Chen, L. Chen, Chem. Eng. J. **358**, 891 (2019).
[26] P. Liu, R. Bao, D. Fang, J. Yi, L. Li, Adv. Powder Technol. **29**, 2027 (2018).
[27] K. Xu, H. Yan, C.F. Tan, Y. Lu, Y. Li, G.W. Ho, R. Ji, M. Hong, Adv. Opt. Mater. **6**, 1701167 (2018).
[28] J. Wang, H. Xu, X. Qian, Y. Dong, J. Gao, G. Qian, J. Yao, Chem. Asian J. **10**, 1276 (2015).
[29] Y. Duan, Y. Shen, Water Sci. Technol. **76**, 172 (2017).

*Corresponding author: xjzhang@hyit.edu.cn